ARTICLE

Radial Elasticity of Self-Assembled Lipid Tubules

Yue Zhao, Karan Tamhane, Xuejun Zhang, Linan An, and Jiyu Fang*

Advanced Materials Processing and Analysis Center and Department of Mechanical, Materials, and Aerospace Engineering, University of Central Florida, Orlando, Florida 32816

ABSTRACT Self-assembled lipid tubules with crystalline bilayer walls represent useful supramolecular architectures which hold promise as vehicles for the controlled release of preloaded drugs and templates for the synthesis of one-dimensional inorganic materials. We study the local elasticity of lipid tubules of 1,2-bis(tricosa-10,12-diynoyl)-*sn*-glycero-3-phosphocholine by radial atomic force microscope indentation, coupled with finite element analysis. A reduced stiffness is found to extend a distance of ~600 nm from the ends of lipid tubules. The middle section of lipid tubules is homogeneous in terms of their radial elasticity with a Young's modulus of ~703 MPa. The inhomogeneous radial elasticity likely arises from the variation of lipid packing density near the tubule ends.

KEYWORDS: lipid tubules · atomic force microscopy · finite element analysis · nanomechanics

Lipids are able to self-assemble into a variety of supramolecular structures with well-defined shapes in solutions.[1,2] Spherical vesicles are the most common self-assembled structure of lipids, which have been extensively studied.[3] Recently, a number of synthetic lipids with modified headgroups or acyl chains have shown the ability to self-assemble into hollow cylindrical tubule structures with diameters from 10 nm to 2.0 μm, depending on the nature of lipids and the conditions under which molecular self-assembly occurs.[4–6] For example, lipid tubules with a characteristic diameter of ~500 nm could be formed in solutions by cooling the lipid bilayers of 1,2-bis(tricosa-10,12-diynoyl)-*sn*-glycero-3-phosphocholine ($DC_{8,9}PC$) from the disordered L_α phase into an ordered $L_{\beta'}$ gel phase.[7] $DC_{8,9}PC$ tubules formed in ethanol/water solution typically have 10 bilayer walls.[8] Unlike spherical vesicles, cylindrical tubules reflect the chiral nature of the $DC_{8,9}PC$.[9] The well-ordered and crystalline packing of the acyl chains in $DC_{8,9}PC$ tubules has been well-characterized.[10–13] The lipid tubules with crystalline bilayer walls and hydrophilic surfaces have shown promise as vehicles for the controlled release of preloaded drugs[14–16] and templates for the synthesis of metallic and silica cylinders,[17–22] as well as provide confined aqueous environments for the encapsulation of functional molecules.[23–26]

The rigidity of self-assembled lipid tubules is a key factor that has a strong impact in their applications. For example, if lipid tubules are to be used as controlled release vehicles for injection in blood vessels, they must sustain the flow of blood circulation. The instability of tubule vehicles under the blood flow will affect the release rate of preloaded drugs. For metallization applications, the rigidity of lipid tubules determines whether they can be used as a template. If lipid tubules are too soft, then they are too fragile to be coated in the metallization. Furthermore, the elasticity of lipid bilayers also determines their shape and mechanical stability.[27] In terms of molecular structures, the acyl chains of lipids freeze in a nearly all-*trans* configuration, and the lipid molecules are arranged in a crystalline lattice in the $L_{\beta'}$ gel phase of lipid tubules. Conversely, in the fluidic L_α phase of lipid vesicles, the "melted" acyl chains are positional disorder in the bilayer walls. The knowledge of mechanical behaviors of lipid tubules can also help us to understand the principle underlying the mechanical behavior of cell membranes. Recently, the axial stiffness of lipid tubules was studied with optical tweezers[28] and the interface tension of moving liquid droplets.[29,30] The axial Young's modulus of lipid tubules made of cardanyl-β-D-glucopyranoside with a diameter of ~50 nm was found to be ~720 MPa.[28] While $DC_{8,9}PC$ lipid tubules with a diameter of ~500 nm showed an axial Young's modulus of ~1.07 GPa.[30]

*Address correspondence to jfang@mail.ucf.edu.

Received for review December 2, 2007 and accepted June 16, 2008.

Published online July 22, 2008.
10.1021/nn8001517 CCC: $40.75

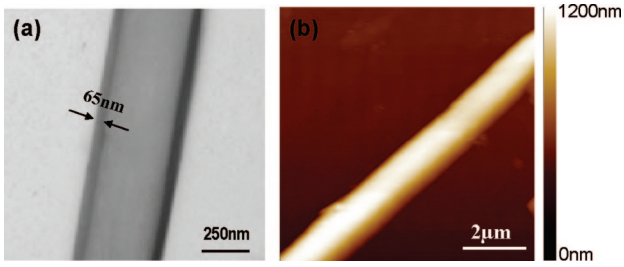

Figure 1. (a) TEM image of a $DC_{8,9}PC$ lipid tubule dried on a carbon-coated grid and (b) AFM image of a $DC_{8,9}PC$ lipid tubule adsorbed on a glass substrate. The TEM image was taken at room temperature. The AFM image was taken with the silicon nitride AFM tip in a liquid cell at room temperature.

Atomic force microscopy (AFM) has proved its value as an indenter for studying the nanomechanics of lipid vesicles,[31–33] virus capsids,[34–40] and protein nanotubes[41–48] by collecting force−distance curves over a point on their surfaces. Through the analysis of the force−distance curves with appropriate theoretical models, quantitative information can be obtained regarding their elastic properties such as stiffness and Young's modulus. The advantage of AFM-based indentation includes its high sensitivity in applying and measuring forces, high precision in positioning a tip relative to the samples, and ability to operate in physiological environments. In this paper, we study the local elasticity of $DC_{8,9}PC$ tubules along the longitudinal direction by radial AFM indentation operating in contact mode in a liquid cell, coupled with finite element analysis.

RESULTS AND DISCUSSION

Figure 1a is a transmission electron microscopy (TEM) image of a $DC_{8,9}PC$ lipid tubule placed on a carbon-coated grid. The lipid tubule shows a hollow structure with a wall thickness of ~65 nm, corresponding to a 10 bilayer wall because the thickness of single lipid bilayers in $DC_{8,9}PC$ tubule walls determined by X-ray diffraction is ~6.6 nm.[10] The external diameter of the tubules is ~500 nm. Figure 1b shows an AFM image of a $DC_{8,9}PC$ lipid tubule adsorbed on a glass substrate in a liquid cell. The image was taken with a silicon nitride cantilever tip. The tubule shows a cylindrical shape, suggesting that the tubule is not compressed at the tip force employed for scanning and is grossly distorted by the adsorption on the glass substrate.

Before beginning the indentation experiments, a colloidal AFM tip with a diameter of 600 nm was placed at the top of the tubule under the guidance of an optical microscope built in AFM. The advantage of using the colloidal AFM tip as a force probe lies in its well-defined size and geometry. To better position the colloid AFM tip in the center region of the lipid tubule, the long axial of the AFM cantilever was set to be parallel to the long axis of the tubule (Figure 2). To prevent the force probe from plowing the surface laterally during indentation, and therefore to further prevent the lateral friction force, the X Rotate parameter was set to be 22°. For each indentation measurement, force−*z* pi-

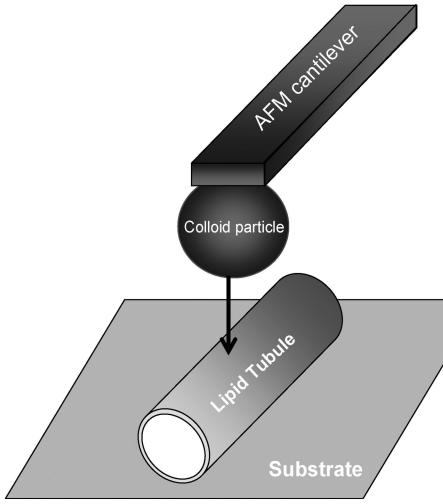

Figure 2. Indenting a lipid tubule adsorbed on a glass substrate with a colloidal AFM tip. The long axial of the AFM cantilever was set to be parallel to the long axis of the tubule to better position the colloid AFM tip in the center region of the lipid tubule.

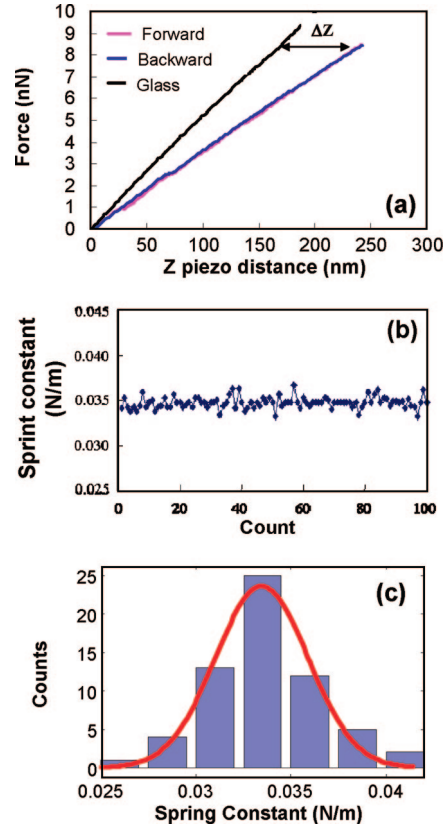

Figure 3. Typical force−*z* piezo distance (FZ) curves of a tubule together with FZ curve on a glass substrate. These FZ curves were performed under AFM contact mode in a liquid cell. (b) Distribution of 100 individual measured point spring constants from the tubule by the same colloid AFM tip. (c) Histogram of measured point spring constants from 62 tubules by three colloid AFM tips with Gaussian distribution.

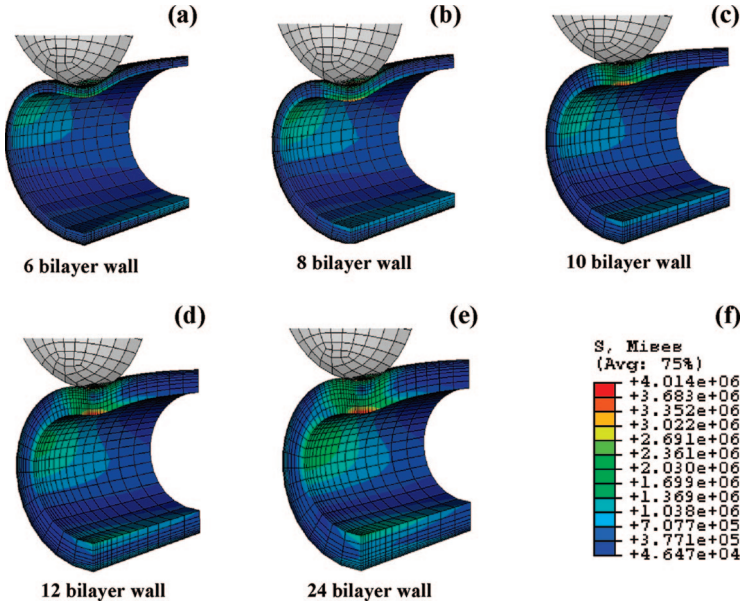

Figure 4. Simulated deformation of the half-segments of modeled tubules with the same external diameter of 500 nm, but different wall thicknesses of 39.6, 52.8, 66.0, 79.2, and 158.4 nm corresponding to 6 (a), 8 (b), 10 (c), 12 (d), and 24 (e) bilayers, respectively, at 75 nm indentation depth. The von Mises stress is indicated by color contours (f).

ezo distance (FZ) curves were performed under AFM contact mode in a liquid cell. Figure 3a is a typical FZ curve (red line) taken on the top of the tubule shown in Figure 1b at a loading rate of 2.54 μm/s, together with the FZ curve (dark line) on the glass substrate, which can be considered as an infinitely stiff material compared to the AFM cantilever. Both FZ curves were obtained with the same cantilever tip. So the change in the sensitivity of the photodiode and the positioning of the laser on the cantilever can be ignored. The FZ curve on the tubule shows no hysteresis when the colloidal AFM tip is retracted at the same speed (blue line), suggesting that the tubule undergoes elastic deformation under the indentation measurement. The horizontal distance (ΔZ) between the FZ curves for a given loading force is the indentation depth of the tubule by the colloidal AFM tip (see Figure 3a). To ensure that the supporting glass substrate does not contribute to the measured elastic properties of lipid tubules, we kept the ΔZ smaller than 75 nm, ~15% of the original tubule diameter. The spring constants (k_{mea}) (stiffness) measured from the slopes of 100 FZ curves on the same tubule with the same cantilever tip show a small standard deviation of 5.8% around the average K_{mea} of 0.0347 N/m. There is no change in the average K_{mea} observed when the loading rate varies from 90 nm/s to 2.54 μm/s. Furthermore, we collected the FZ curves from the center region of 62 lipid tubules with a diameter of 500 ± 10 nm by performing one indentation on each of them. Three colloid AFM tips from the same manufacturer were used for these indentations. The average spring constant (k_{mea}) was given by Gaussian curve fitting to be 0.0347 ± 0.0017 N/m with a standard deviation of ~17% (Figure 3c). The relatively large standard deviation from multiple tubules is likely due to the slight deviation of tubule diameters and cantilever spring constants.

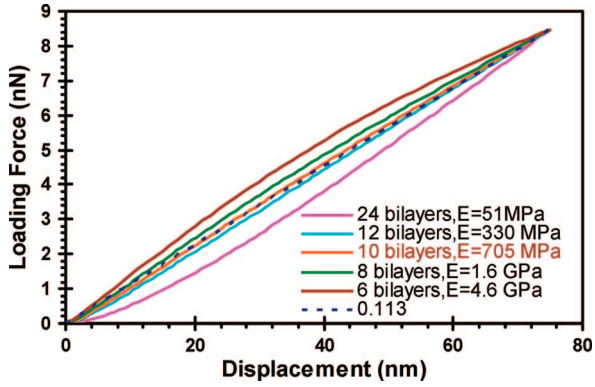

Figure 5. Simulated force−displacement curves (solid lines) of modeled tubules. The external diameter of the modeled tubules was kept at 500 nm, while both the Young's modulus (E) and the number of bilayers in the tubule walls were varied until the simulated curves within 75 nm displacement could be best fitted with the measured spring constant (K_{tub}) of 0.113 N/m (dashed line). The optimized fitting results are (brown) 6 bilayers, E = 4.6 MPa; (green) 8 bilayers, E = 1.6 GPa; (orange) 10 bilayers, E = 705 MPa; (blue) 12 bilayers, E = 330 MPa; and (magenta) 24 bilayers, E = 51 MPa.

The measured point sprint constant (k_{mea}) comprises the spring constants of both the tubules (K_{tub}) and the cantilever (K_{can}). The system can be modeled as two springs arranged in a series. The point spring constant (stiffness) of lipid tubules can be calculated according to Hooke's law: $k_{tub} = k_{can} \times k_{mea}/k_{can} - k_{mea}$. Using the equation, we find that the point spring constant of lipid tubules is 0.113 ± 0.019 N/m.

To calculate the Young's modulus of lipid tubules from the spring constant, we simulated the contact between the colloidal AFM tip and the tubule by the finite-element method with the commercially available package ABAQUS. The tubule was simulated as isotropic cylindrical shells made from a homogeneous material with an external diameter of 500 nm similar to the diameter of the lipid tubules resting on a flat rigid surface and loaded by a rigid indenter with a diameter of 600 nm similar to the diameter of the colloidal AFM tip. The AFM tip−lipid tubule and the lipid tubule−rigid substrate contacts are modeled as frictionless. The finite element model allows us to follow the deformation of the tubules as they are indented and determine the local stress in the bilayer walls. Figure 4 shows the deformed shapes of the half-segments of modeled tubules with the same external diameter of 500 nm, but different wall thickness of 39.6, 52.8, 66.0, 79.2, and 158.4 nm, corresponding to 6, 8, 10, 12, and 24 bilayers, respectively. Although, the typical wall thickness is 10 bilayers for the $DC_{8,9}PC$ tubules formed in ethanol/water solution, TEM analysis also reveals the presence of a small number of tubules with 6, 8, 12, and 24 bilay-

ers. AFM allows us to measure the external diameter of imaged lipid tubules but provides no information on the wall thickness. The color shown in these deformed tubules is an indication of the von Mises stress (Figure 4f). During the simulation process, we varied both the Young's modulus and the wall thickness until the simulated force−indentation curves are best fitted with the spring constant (K_{tub}) of 0.113 N/m. As can be seen from the optimized fitting results for each modeled tubule shown in Figure 5, the tubule with a wall thickness of 66 nm and a radial Young's modulus of 703 MP is best fitted with the spring constant. The simulation also shows that 2% variation in the tubule diameter does not affect the fitting results. The calculated radial Young's modulus of the $DC_{8,9}PC$ tubules is slightly lower than the axial Young's modulus (1.07 GPa) measured from bending experiments.[30] In our measurements, the indentation depth was kept to be smaller than 75 nm, ~15% of the original tubule diameter. Also, the simulation shows that, at 75 nm indentation depth, the stress concentrates in the upper region of the lipid tubule (Figure 4). The effect of the supporting glass substrate on the measured elastic properties of lipid tubules can be ignored. We believed that the difference between the radial and axial modulus is a result of the anisotropic interaction of lipid molecules in multibilayer walls. Furthermore, it has been shown that the acyl chains of lipid molecules in multibilayer walls are tilted with respect to the equator of $DC_{8,9}PC$ tubules.[49] The photopolymerization of the diacetylenic groups placed at the center of the acyl chains is expected to strengthen the lateral chain−chain interaction, leading to the increase of the axial stiffness of tubules.

We are interested in comparing the Young's modulus of $DC_{8,9}PC$ tubules with those of other self-assembled lipid structures. It is known that the lipid molecules in the $L_{\beta'}$ gel phase of crystalline lipid tubules cannot move as freely as in the fluidic L_{α} phase of lipid vesicles. So the mechanical properties of crystalline lipid tubules, such as the compressibility and bending rigidity, are expected to differ from that of fluidic lipid vesicles. The radial Young's modulus of $DC_{8,9}PC$ lipid tubules (703 MPa) is significantly larger than those reported on cholinergic synaptic lipid vesicles (0.2−1.3 MPa),[31] egg-PC lipid vesicles (1.97 MPa),[32] and DPPC vesicles (110 MPa).[33]

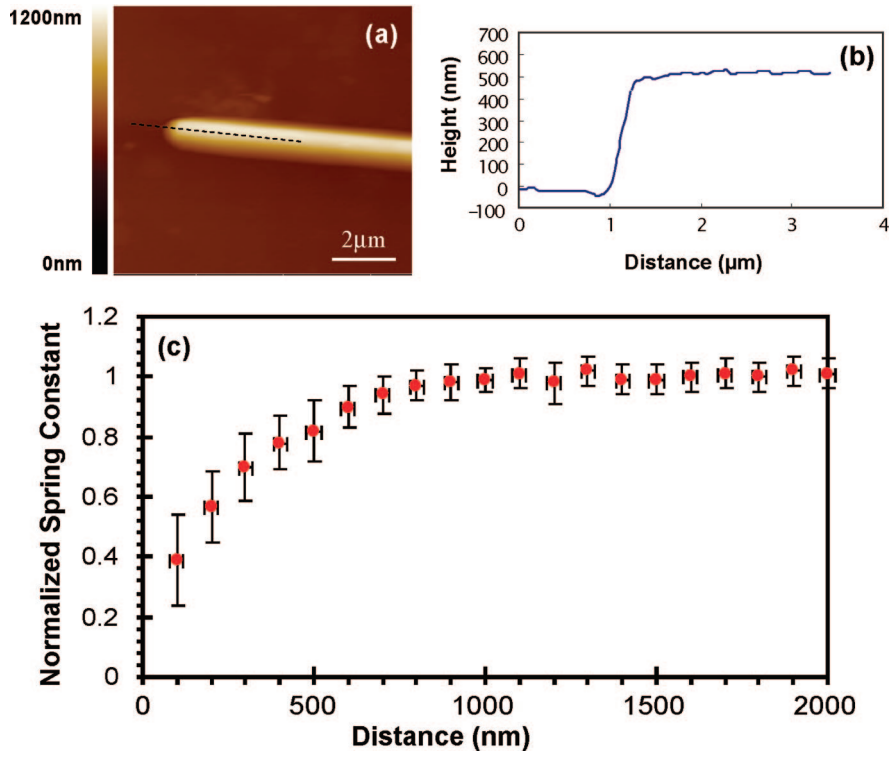

Figure 6. (a) AFM image of a $DC_{8,9}PC$ tubule on a glass substrate. One end of the tubule is visible. (b) High profile along the dashed line shown in panel a suggests that the tubule has a constant diameter near its end. (c) Normalized spring constant as a function of distance from the tubule end. Reduced spring constants were observed over a distance of ~600 nm from the tubule end. Both the AFM image and the indentation measurements were taken with the same silicon nitride AFM tip.

By using a silicon nitride AFM tip as a force probe, we carry out the indentation near the ends of lipid tubules. The benefit of using the small silicon nitride AFM tip is that the indentation position along the lipid tubules can be relatively easy to control. Figure 6a is an AFM image taken near one end of a lipid tubule on a glass substrate in a liquid cell. The high profile along the longitudinal direction suggests that the tubule has a constant height (~500 nm) near its end (Figure 6b). A series of positioned indenta-

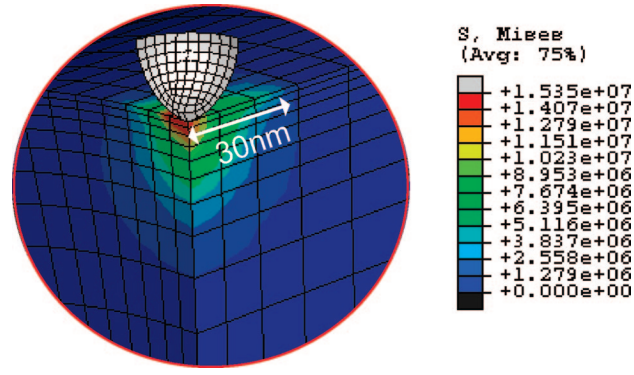

Figure 7. Simulated deformation of one-quarter of the modeled tubule with an external diameter of 500 nm and a wall thickness of 66 nm at an indentation of 27 nm. The von Mises stress is indicated by color contours. The deformed region under the silicon nitride AFM tip indentation extends to both sides for ~30 nm.

tions were carried out from the end of the tubule to the middle section with the same silicon nitride AFM tip. Five indentations were preformed at each position. Figure 6c is a plot of the measured spring constants normalized to the value obtained on the tubule far from the end as a function of the distance along the longitudinal direction. Exact determination of the indentation position is difficult from experiments due to the thermal drift. In our experiments, the thermal drift of the AFM indentation was estimated by imaging a lipid tubule adsorbed on a glass substrate over time at a scanning speed of 0.3 μm/s to be less than 20 nm (<4% of the original tubule diameter). To precisely control indentation positions, we lowered the scanning speed to 0.3 μm/s and gradually reduced the scanning areas to within 30 nm × 30 nm. The error bars in the distance reflect the uncertainty in measuring the indentation positions along the longitudinal direction. Interestingly, we find that the reduced stiffness extends a distance of ~600 nm from the tubule end (see Figure 6c).

Under the point indentation, the deformation of lipid tubules is expected to extend to both sides at the longitudinal direction. Figure 7 shows the finite element model of the contact between the silicon nitride AFM tip with a radius of 15 nm and the lipid tubule with a 500 nm diameter and a 10 lipid bilayer wall. The deformed region of the modeled tubule under the point indentation extends to both sides along the long axis for ~30 nm. Due to the symmetry break of the deformation at the end of the tubule, we expect that the end effect is in the distance less than ~30 nm, which is much smaller than the extension of the reduced stiffness from the tubule end (~600 nm).

There are several issues to be considered when we are interpreting the reduced stiffness near the ends of lipid tubules. The indentation along the longitudinal direction was carried out with the same silicon nitride tips. The influence of tip sizes and cantilever spring constants on the measured stiffness can be limited. It is known that lipid tubules are formed by rolled-up bilayer sheets. The decrease of the number of bilayers in tubule walls can lead to the decrease of the stiffness of lipid tubules.[29] However, there is no bilayer edge with a 6.5 nm height observed on the tubule surface. The high profile (Figure 6b) shows that the tubule has a uniform diameter near its end. So the influence of changing the tubule diameter on the measured stiffness can be ruled out. The thermal drift of indentation positions away from the center of the tubule may cause the variation of the measured spring constants. It was shown that the measured spring constants of polyelectrolyte tubules increased when the indentation positions are away from their center region (pole region).[50] To exam the effect of the thermal drift on

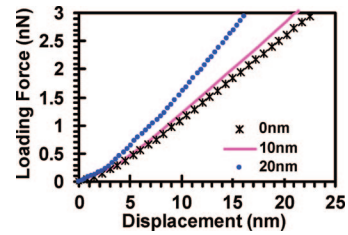

Figure 8. Simulated force−displacement curves at the shift of 0 nm (*), 10 nm (—), and 20 nm (●) away from the center of a modeled tubule with an external diameter of 500 nm and a wall thickness of 66 nm.

the measured stiffness, we modeled the force−displacement curves at the drift of 0, 10, and 20 nm away from the center of a lipid tubule with a 500 nm diameter and a 10 lipid bilayer wall (Figure 8). At small displacements (<3 nm), there is no difference in the calculated slopes (spring constant) at these three positions. At larger indentations, the discrepancy in the calculated spring constants (slopes) becomes visible when the probing position is away from the center. The change of calculated spring constants with respect to the tubule center is found to be 0.01 N/m for 10 nm drift and 0.06 N/m for 20 nm drift. The variation (error bar) of the measured spring constants at each position during the multiple indentations (Figure 6c) is believed to be the result of the thermal drift of the indentation positions away from the tubule center. Even after taking into account these variations, the decrease of the measured average spring constant near the end of the tubule is still evident. The reduced spring constant might arise from the variation of the lipid packing near the tubule ends. The selective adsorption of charged nanoparticles at the ends of the $DC_{8,9}PC$ tubules has suggested that the lipid packing is not perfect at the tubule ends.[51] The fluorescence recovery after photobleaching has shown that the diffusion of Nile red (a hydrophobic probe) in the bilayer walls of $DC_{8,9}PC$ tubules slows down at the middle while it becomes faster at the ends.[52] This result also suggests that the packing density of lipid molecules at the tubule ends is lower than that in the middle. So it is likely that the variation of lipid packing in tubule walls leads to the reduced stiffness near the ends of the lipid tubules.

In conclusion, the local elasticity of $DC_{8,9}PC$ lipid tubules has been studied by AFM-based radial indentation, coupled with finite element analysis. We find that a reduced radial stiffness extends ~600 nm from the ends of lipid tubules. The middle section of the lipid tubules is homogeneous with a radial Young's modulus of 703 MPa. The reduced radial stiffness might reflect the change of lipid packing density near the tubule ends.

MATERIALS AND METHODS

Lipid tubules were synthesized by thermal cycling of a 5 mg/mL suspension of 1,2-bis(tricosa-10,12-diynoyl)-*sn*-glycero-3-phosphocholine ($DC_{8,9}PC$) (Avanti Polar Lipids, Alabaster, AL) in ethanol/water (70:30 v/v) from 60 °C to room temperature at a rate of ~0.5 °C/min.[7] The polymerization of lipid tubules in solutions was performed with a UV light (254 nm) for 20 min at room temperature. Atomic force microscopy (AFM) (Dimension 3100, Digital Instruments) with an opened loop scanner and software version 6.12r1 was used to study the structure and mechanical properties of lipid tubules absorbed on glass slides in a liquid cell. Silicon nitride cantilevers (Nanosensors) with a spring constant of 0.051 N/m (given by the manufacturer) were employed in imaging lipid tubules. The size of the cantilever tips (radius of curvature) is about 15 nm according to the manufacturer. AFM images of lipid tubules were obtained in contact mode at a scanning rate of 0.5 Hz and a 512 × 512 pixel size. Indentation experiments of lipid tubules on glass slides were conducted with a colloid probe−AFM technique in a liquid cell at room temperature. In this technique, a silica colloidal particle with a diameter of ~600 nm was mounted onto a tipless AFM cantilever (Novascan Technologies, Inc.). The benefit of using colloidal particles as a force probe lies in obtaining a well-defined geometry. To carry out the indentation near the ends of lipid tubules, the silicon nitride tip with a radius of 15 nm was used as an indenter. Transmission electron microscopic measurements of lipid tubules on carbon-coated grids were performed on a Tecnai F30 microscope with an accelerating voltage of 300 kV at room temperature.

The Young's modulus was calculated from the measured stiffness of lipid tubules with finite element method. In the finite element simulation process, the lipid tubules were modeled as a tubule made of a homogeneous material, sitting on a flat rigid surface and loaded by a spherical rigid indenter. The Poisson ratio of lipid tubules is taken as 0.48, a mean value of common biomaterials. Considering the axial symmetry of the problem, the model was reduced to a quarter sector using the two mirror symmetry planes intersecting at the loading point. This quarter sector was divided into 4500 brick elements and subjected to axisymmetrical boundary conditions. The postprocessing was done by ABAQUS-6.6 software. Loading was simulated by prescribing the downward movement of the rigid indenter, calculated in 100 increments.

Acknowledgment. This work is supported by the National Science Foundation (CMMI 0726478).

REFERENCES AND NOTES

1. Israelachvili J. *Intermolecular and Surface Force*; Academic Press: San Diego, CA, 1992.
2. Collier, J. H.; Messersmith, P. B. Phospholipid Strategies in Biomineralization and Biomaterials Research. *Annu. Rev. Mater. Res.* **2001**, *31*, 237–263.
3. Lipowaky, R.; Sackmann, E. *Structure and Dynamics of Membranes*; Elsevier: Amsterdam, 1995.
4. Spector, M. S.; Selinger, J. V.; Schnur, J. M. In *Materials-Chirality: Vol. 24 of Topics in Stereochemistry: Chiral Molecular Self-Assembly*; Green, M. M., Nolte, R. J. M., Meijer, E. W., Eds.; Wiley: Hoboken, NJ, 2003.
5. Shimizu, T.; Masuda, M.; Minamikawa, H. Supramolecular Nanotube Architectures Based on Amphiphilic Molecules. *Chem. Rev.* **2005**, *105*, 1401–1444.
6. Fang, J. Y. Ordered Arrays of Self-Assembled Lipid Tubules: Fabrication and Applications. *J. Mater. Chem.* **2007**, *17*, 3479–3484.
7. Yager, P.; Schoen, P. E. Formation of Tubules by a Polymerizable Surfactant. *Mol. Cryst. Liq. Cryst.* **1984**, *106*, 371–381.
8. Ratna, B. R.; Baral-Tosch, S.; Kahn, B.; Rudolph, A. S.; Schnur, J. M. Effect of Alcohol Chain-Length on Tubule Formation of 1,2-Bis(tricosa-10,12-diynoyl)-*sn*-glycero-3-phosphocholine. *Chem. Phys. Lipids* **1992**, *63*, 47–53.
9. Spector, M. S.; Price, R. R.; Schnur, J. M. Chiral Lipid Tubules. *Adv. Mater.* **1999**, *11*, 337–340.
10. Thomas, B. N.; Safinya, C. R.; Plano, R. J.; Clark, N. A. Lipid Tubule Self-Assembly-Length Dependence on Cooling Rate through a First-Ordered Phase-Transition. *Science* **1995**, *267*, 1635–1638.
11. Rudolph, A. S.; Singh, B. P.; Singh, A.; Burke, T. G. Phase Characterization of Positional Isomers 1,2-Di(heptacosadiynoyl)-*sn*-glycero-3-phosphochomine-Tubule Forming Phosphatidylcholines. *Biochim. Biophys. Acta* **1988**, *943*, 454–462.
12. Lando, J. B.; Sudiwiala, R. V. Structural Investigation of Langmuir−Blodgett Films and Tubules of 1,2-Bis(tricosa-10,12-diynoyl)-*sn*-glycero-3-phosphocholine using Electron-Diffraction Techniques. *Chem. Mater.* **1990**, *2*, 594–599.
13. Mahajan, N.; Zhao, Y.; Du, T.; Fang, J. Y. Nanoscale Ripples in Self-Assembled Lipid Tubules. *Langmuir* **2006**, *22*, 1973–1975.
14. Schnur, J. M.; Price, R. R.; Rudolph, A. S. Biologically Engineered Microstructures-Controlled Released Application. *J. Controlled Release* **1994**, *28*, 3–13.
15. Goldstein, A. S.; Gelb, M. H.; Yager, P. Continuous and Highly Variable Rate Controlled Release of Model Drugs from Sphingolipid-Based Complex High Axial Ratio Microstructures. *J. Controlled Release* **2001**, *70*, 125–138.
16. Meilander, N. J.; Pasumarthy, M. K.; Kowalczyk, T. H.; Cooper, M. J.; Bellamkonda, R. V. Sustained Release of Plasmid DNA Using Lipid Microtubules and Agarose Hydrogel. *J. Controlled Release* **2003**, *88*, 321–331.
17. Baral, S.; Schoen, P. Silica-Deposited Phospholipid Tubules as a Precursor to Hollow Submicron-Diameter Silica Cylinders. *Chem. Meter.* **1993**, *5*, 145–147.
18. Price, R. R.; Dressick, W. J.; Singh, A. Fabrication of Nanoscale Metallic Spirals Using Phospholipid Microtubule Organizational Templates. *J. Am. Chem. Soc.* **2003**, *125*, 11259–11263.
19. Patil, A. J.; Muthusamy, E.; Seddon, A. M.; Mann, S. Higher-Order Synthesis of Organoclay Pipes Using Self-Assembled Lipid Templates. *Adv. Mater.* **2003**, *15*, 1816–1819.
20. Jung, J. H.; Lee, S. H.; Yoo, J. S.; Yoshida, K.; Shimizu, T.; Shinkai, S. Creation of Double Silica Nanotubes by Using Crown-Appended Cholesterol Nanotubes. *Chem.—Eur. J.* **2003**, *9*, 5307–5313.
21. Zhou, Y.; Ji, Q.; Masuda, M.; Kamiya, S.; Shimizu, T. Helical Arrays of CdS Nanoparticles Tracing on a Functionalized Chiral Template of Glycolipid Nanotubes. *Chem. Mater.* **2006**, *18*, 403–406.
22. Zhao, Y.; Liu, J.; Sohn, Y.; Fang, J. Y. Synthesis of Stable Hybrid Silica-Lipid Cylinders with Nanoscale Helical Ripples. *J. Phys. Chem. C* **2007**, *111*, 6418–6421.
23. Kameta, N.; Masuda, M.; Minamikawa, H.; Goutev, N. V.; Rim, J. A.; Jung, J. H.; Shimizu, T. Selective Construction of Supramolecular Nanotube Hosts with Cationic Inner Surfaces. *Adv. Mater.* **2005**, *17*, 2732–2736.
24. Yu, L.; Banerjee, I. A.; Gao, X.; Nuraje, N.; Matsui, H. Fabrication and Application of Enzyme-Incorporated Peptide Nanotubes. *Bioconjugate Chem.* **2005**, *16*, 1484–1487.
25. Zhao, Y.; Mahaja, N.; Fang, J. Y. Self-Assembled Cylindrical Lipid Tubules with a Birefringent Core. *Small* **2006**, *2*, 364–367.
26. Kameta, N.; Masuda, M.; Minamikawa, H.; Mishima, Y.; Yamashita, I.; Shimizu, T. Functionalizable Organic Nanochannels Based on Lipid Nanotubes: Encapsulation and Nanofluidic Behavior of Biomacromolecules. *Chem. Mater.* **2007**, *19*, 3553–3560.
27. Selinger, R. L. B.; Selinger, J. V.; Malanoski, A. P.; Schnur, J. M. Shape Selection in Chiral Self-Assembly. *Phys. Rev. Lett.* **2004**, *93*, 158103.
28. Frusawa, H.; Fukagawa, A.; Ikeda, Y.; Araki, J. A.; Ito, K.; John, G.; Shimizu, T. Aligning a Single-Lipid Nanotube with Moderate Stiffness. *Angew. Chem., Int. Ed.* **2003**, *42*, 72–74.
29. Zhao, Y.; Mahajan, N.; Fang, J. Y. Bending and Radial Deformation of Lipid Tubules on Self-Assembled Thiol Monolayers. *J. Phys. Chem. B* **2006**, *110*, 22060–22063.

30. Zhao, Y.; An, L.; Fang, J. Y. Buckling of Lipid Tubules in Shrinking Liquid Droplets. *Nano Lett.* **2007**, *7*, 1360–1363.
31. Laney, D. E.; Garcia, R. A.; Parsons, S. M.; Hansma, H. G. Changes in the Elastic Properties of Cholinergic Synaptic Vesicles as Measured by Atomic Force Microscopy. *Biophys. J.* **1997**, *72*, 806–813.
32. Ling, X.; Mao, G.; Simon Ng, K. Y. Mechanical Properties and Stability Measurement of Cholesterol-Containing Liposome on Mica by Atomic Force Microscopy. *J. Colloid Interface Sci.* **2004**, *278*, 53–62.
33. Delorme, N.; Fery, A. Direct Method to Study Membrane Rigidity of Small Vesicles Based on Atomic Force Microscopy Spectroscopy. *Phys. Rev. E* **2006**, *74*, 030901(R)
34. Ivanovska, I. L.; de Pablo, P. J.; Ibarra, B.; Sgalari, G.; Mackintosh, F. C.; Carrascoa, J. L.; Schmidt, C. F.; Wuite, G. J. L. Bacteriophage Capsids: Tough Nanoshells with Complex Elastic Properties. *Proc. Natl. Acad. Sci. U.S.A.* **2004**, *101*, 7600–7605.
35. Michel, J. P.; Ivanovska, I. L.; Gibbons, M. M.; Klug, W. S.; Knobler, C. M.; Wuite, G. J. L.; Schmidt, C. F. Nanoindentation Studies of Full and Empty Viral Capsids and the Effects of Capsid Protein Mutations on Elasticity and Strength. *Proc. Natl. Acad. Sci. U.S.A.* **2006**, *103*, 6184–1689.
36. Klug, W. S.; Bruinsma, R. F.; Michel, J. P.; Knobler, C. M.; Ivanovska, I. L.; Schmidt, C. F.; Wuite, G. J. L. Failure of Viral Shells. *Phys. Rev. Lett.* **2006**, *97*, 228101.
37. Carrasco, C.; Carreira, A.; Schaap, I. A. T.; Serena, P. A.; Gomez-Herrero, J; Mateu, M. G.; De Pablo, P. J. DNA-Mediated Anisotropic Mechanical Reinforcement of a Virus. *Proc. Natl. Acad. Sci. U.S.A.* **2006**, *103*, 13706–13711.
38. Zhao, Y.; Mahajan, N.; Long, S.; Wang, Q.; Fang, J. Y. Stability of Virus Nanoparticles on Substrates under Applied Load with Atomic Force Microscope. *Micro. Nano Lett.* **2006**, *1*, 1–3.
39. Kol, N.; Gladnikoff, M.; Barlam, D.; Shneck, R. Z.; Rein, A.; Rousso, I. Mechanical Properties of Murine Leukemia Virus Particles: Effect of Maturation. *Biophys. J.* **2006**, *91*, 767–774.
40. Gibbons, M. M.; Klug, W. S. Nonlinear Finite-Element Analysis of Nanoindentation of Viral Capsids. *Phys. Rev. E* **2007**, *75*, 031901.
41. de Pablo, P. J.; Schaap, I. A. T.; MacKintosh, F. C.; Schmidt, C. F. Deformation and Collapse of Microtubules on the Nanometer Scale. *Phys. Rev. Lett.* **2003**, *91*, 098101.
42. Kis, A.; Kasas, S.; Babić, B.; Kulik, A. J.; Benoît, W.; Briggs, G. A. D.; Schönenberger, C.; Catsicas, S.; Forró, L. Nanomechanics of Microtubules. *Phys. Rev. Lett.* **2002**, *89*, 248101.
43. Kol, N.; Adler-Abramovich, L.; Barlam, D.; Shneck, R. Z.; Gazit, E.; Rousso, I. Self-Assembled Peptide Nanotubes are Uniquely Rigid Bioinspired Supramolecular Structures. *Nano Lett.* **2005**, *5*, 1343–1346.
44. Graveland-Bikker, J. F.; Schaap, I. A. T.; Schmidt, C. F.; de Kruif, C. G. Structural and Mechanical Study of a Self-Assembling Protein Nanotube. *Nano Lett.* **2006**, *6*, 616–621.
45. Schaap, I. A. T.; Carrasco, C.; de Pablo, P. J.; Mackintosh, F. C.; Schmidt, C. F. Elastic Response, Buckling, and Instability of Microtubules under Radial Indentation. *Biophys. J.* **2006**, *91*, 1521–1531.
46. Smith, J. F.; Knowles, T. P. J.; Bobson, C. M.; MacPhee, C. E.; Welland, M. E. Characterization of the Nanoscale Properties of Individual Amyloid Fibrils. *Proc. Natl. Acad. Sci. U.S.A.* **2006**, *103*, 15806–15811.
47. Niu, L.; Chen, X.; Allen, S.; Tendler, S. J. B. Using the Bending Beam Model to Estimate the Elasticity of Diphenylalanine Nanotubes. *Langmuir* **2007**, *23*, 7443–7446.
48. Munson, K. M.; Mulugeta, P. G.; Donhauser, Z. J. Enhanced Mechanical Stability of Microtubules Polymerized with a Slowly Hydrolyzable Nucleotide Analogue. *J. Phys. Chem. B* **2007**, *111*, 5053–5057.
49. Zhao, Y.; Mahajan, N.; Lu, R.; Fang, J. Y. Liquid-Crystal Imaging of Molecular-Tilt Ordering in Self-Assembled Lipid Tubules. *Proc. Natl. Acad. Sci. U.S.A.* **2005**, *102*, 7438–7442.
50. Mueller, R.; Daehne, L.; Fery, A. Hollow Polyelectrolyte Multilayer Tubes: Mechanical Properties and Shape Changes. *J. Phys. Chem. B* **2007**, *111*, 8547–8553.
51. Lvov, Y. M.; Price, R. R.; Selinger, J. V.; Singh, A.; Spector, M. S.; Schnur, J. M. Imaging Nanoscale Patterns on Biologically Derived Microstructures. *Langmuir* **2000**, *16*, 5932–5935.
52. Guo, L.; Chowdhury, P.; Fang, J. Y.; Gai, F. Heterogeneous and Anomalous Diffusion inside Lipid Tubules. *J. Phys. Chem. B.* **2007**, *111*, 14244–14249.